Am J Cancer Res 2022;12(4):1843-1854
www.ajcr.us /ISSN:2156-6976/ajcr0131050

Original Article

Signature of the vascular tumor microenvironment as a marker of the therapeutic response to doxorubicin in a preclinical model of osteosarcoma

Vincent Crenn[1,2,3], Jérôme Amiaud[1,2], Anne Gomez-Brouchet[4], Vincent Potiron[5,6], François Gouin[7], Philippe Rosset[8], Louis-Romée Le Nail[8], Luciano Vidal[1,9], Helios Bertin[1,2,10], Régis Brion[1,2], Guillaume Tran[3], Franck Verrecchia[1,2], Isabelle Corre[1,2], Françoise Redini[1,2]

[1]Nantes University, INSERM UMR 1238, Nantes, France; [2]Faculty of Medicine, University of Nantes, Nantes, France; [3]Department of Orthopedics, University Hospital Center Hôtel Dieu, Nantes, France; [4]Department of Anatomical Pathology, University Hospital Center of Purpan, Toulouse, France; [5]CRCINA, INSERM, University of Angers, University of Nantes, Nantes, France; [6]Institut de Cancérologie de l'Ouest, Saint-Herblain, France; [7]Department of Surgery, Léon-Bérard Center, Lyon, France; [8]Department of Orthopedics, Trousseau University Hospital Center, Tours, France; [9]Ecole Centrale Nantes, Rapid Manufacturing Platform, GEM UMR 6183 CNRS Laboratory, Nantes, France; [10]Department of Maxillofacial Surgery, University Hospital Center Hôtel Dieu, Nantes, France

Received January 29, 2021; Accepted September 27, 2021; Epub April 15, 2022; Published April 30, 2022

Abstract: Predicting a response of osteosarcoma patients to chemotherapy, such as doxorubicin or high-dose methotrexate cocktail, remains a challenge in the clinic. Moreover, the prognostic value of currently used necrosis analysis is debatable. New markers of the therapeutic response or the prognostic response are urgently needed. The microenvironment plays a key role in the vascularization of highly heterogeneous tumors. Using the syngeneic MOS-J mouse model of osteosarcoma, we focused our study on the immunohistochemistry of tumor vascularization in order to identify new vessel markers, and to search for potential markers of the therapeutic response. Endomucin+, CD31+, and α-SMA+-positive elements were quantified in control (n=6) and doxorubicin-treated (n=6) mice in three different intra-tumor locations. We also used co-labeling to assess CD31+/Endomucin+ and CD31+/α-SMA+ co-expression. We identified a central tumor zone with a low vascularization profile for all of these markers. We identified two distinct types of vessels: CD31+/Endomucin+ vessels with a sprouting, neo-angiogenic, interlaced appearance, and CD31+/α-SMA+ vessel with a well-defined, mature structure. Doxorubicin appeared to reduce CD31+ expression in the tumor invasion front. In the doxorubicin-sensitive model, there were four times more CD31+/α-SMA+ elements than in the poorly responsive model. Therefore, we propose a methodology based on immunohistochemistry and multiplexed immunofluorescence to use endomucin as a promising new vascular marker in the osteosarcoma model. Moreover, our results suggest that CD31+/α-SMA+ vessels could be considered to be indicators of vasculature normalization and they may be used as specific markers of a good therapeutic response.

Keywords: Osteosarcoma, microenvironment, vascularization, chemotherapy, CD31, endomucin, α-SMA, immunohistochemistry, immunofluorescence, multiplexing

Introduction

Osteosarcomas (OS), which are derived from mesenchymal bone cells, represent the most common type of malignant primary bone tumor. The annual incidence of osteosarcoma in the general population is 5 cases per million [1]. This tumor type has several histological subtypes [2] (osteoblast, chondroblast, telangiectasia, etc.), as well as a high degree of intratumor histological heterogeneity [3, 4]. The prognostic factors for long-term survival described in the literature comprise the location and the size of the tumor, the presence of metastases, the response to chemotherapy determined by the Huvos and Rosen score, as well as on the quality of the tumor resection [5-7]. Polychemotherapy, before and after carcinologic surgery, is the treatment of choice and associates different drug cocktails depending on the

patient's age (high-dose methotrexate, doxorubicin, ifosfamide, cisplatin, etc.) [8]. Despite these protocols, OS survival rates have not improved for approximately 40 years, with a 5-year survival of approximately 75% for localized forms and 25% for metastatic disease [8]. Moreover, 25% of the patients who respond well to chemotherapy as estimated by the Huvos/Rosen score relapse [9].

Using a preclinical model of OS, we previously demonstrated the tumor environment can play a role in the response to chemotherapy [10]. In the syngeneic MOS-J mouse model, we observed a better anti-tumor response to doxorubicin chemotherapy when the tumor was located at an intraosseous site, whereas the tumors appeared to be refractory to the drug when they developed in paratibial areas in close contact with the periosteum and soft tissues. This result was linked to a clinical hypothesis: patients have a good or poor response to chemotherapy depending on the tumor localization in soft or bone tissue extensions. As doxorubicin is a key treatment of OS for patients over the age of 18, understanding and identifying good response predictors seems crucial. This difference in the therapeutic response according to the environmental context is a key factor in the mechanisms of resistance in clinical oncology. Several aspects of the microenvironment have been reported: the role of immunity and inflammation, supporting tissue, and vascularization. The bone microenvironment is indeed highly specialized, with a complex and dynamic environment involving different components: bone cells (osteoclasts, osteoblasts, osteocytes), stromal cells (MSCs, fibroblasts), immune cells (macrophages, lymphocytes), mineralized extracellular matrix (ECM), and vascular cells (endothelial cells and pericytes) [11].

The tumor vasculature is largely determined by angiogenesis. This process is a hallmark of cancer, and the angiogenic switch is one of the main underlying factors of tumor growth [12]. Compared to the normal vasculature, the tumor vascular network is rather immature and dysfunctional. Therefore, it impacts the microenvironment, resulting in hypoxia, acidosis, and glucose starvation, as well as decreasing immune cell infiltration and activity, all of which enable cancer progression, metastasis, and drug resistance. Poor perfusion and an immature tumor vasculature prevent drugs from reaching tumor cells at a lethal concentration [13]. The distribution of chemotherapy drugs in tumor tissues depends on the plasma pharmacokinetics, but the abnormal architecture and functionality of the tumor vessels do not allow optimal distribution of chemotherapeutic agents [14]. These considerations lead to a double-edged sword in therapies when addressing the tumor vasculature: on one hand, blocking neo-vascularization with anti-angiogenic agents to limit tumor expansion, and, on the other hand, preserving functional vessels to deliver drugs in direct contact with the tumor [15].

The vasculature of normal bone during growth has recently been described by Adams's team [16-18], with the characterization of endomucin+ CD31+ type-H vessels in the metaphysis in contact with osteoprogenitors, and type L vessels in the diaphysis. Regarding OS, a detailed characterization of the tumor vascular compartment is lacking and it remains largely unexplored. Drug distribution to the tumor can be considered to be an important factor in poor responses to chemotherapy [14]. There is, therefore a need to focus on OS vascularization. In this context, we analyzed the vascular network of the OS environment in the syngeneic MOS-J orthotopic mouse model of OS, with and without treatment with the chemotherapeutic drug doxorubicin. We examined different areas (invasion front, direct bone contact, and tumor center) in order to refine the analysis of the vascularization architecture according to the geography and to take into account the high degree of heterogeneity of the tumor. We studied expression of the vascular markers CD31, endomucin, and α-SMA by IHC staining. We then studied the distribution of CD31+/Endomucin+ and CD31+/α-SMA+ elements by immunofluorescence multiplexing. We also hypothesized that the tumor vascular signature could be modified by exposure to doxorubicin and that it can also be an indicator of the response to chemotherapy, discriminating good versus poor responders.

Materials and methods

Cell culture

The murine MOS-J osteosarcoma cell line was developed from a spontaneous OS in the

C57BL/6J mouse strain. All of the experiments were performed under sterile conditions using a vertical laminar flow hood (PSM Securiplus, Astec, France). The cells were grown in 25, 75, or 175 cm^2 flasks (Falcon™, Becton Dickinson Labware, NJ, USA) in RPMI 1640 (Roswell Park Memorial Institute, BioWhittaker, Verviers, Belgium) culture medium supplemented with 5% FCS (Fetal Calf Serum, HyClone™, Perbio, Vigneux, France). Plates were seeded at a density of 10^4 cells/cm^2 and were then incubated in a saturated-humidity atmosphere containing 5% CO_2 at 37°C. For subculturing, the cells were detached at confluence with a solution of trypsin-EDTA [BioWhittaker, Trypsin: 0.5 g/L; EDTA (ethylenediaminetetraacetic acid): 0.5 g/L]. The trypsin was neutralized by adding FCS (10% in the culture medium) and the cells were then centrifuged at 1,600 rpm for 5 minutes. Cell counts were performed using a Malassez chamber. When cell amplification was required for in vivo experiments, the MOS-J cells were detached when they were 70-80% confluent in order to achieve optimal comparable growth rates from one procedure to the next.

Murine model

The animal experiments were carried out at the Experimental Therapeutics Unit (Nantes Medical School; accreditation number D-440-45) in accordance with protocols approved by the Regional Committee for Ethics in Animal Experimentation (ECAE n° 6) and the Department of Agriculture, under the direction of the investigators authorized to perform the experiments. Four-week-old male C57BL/6J mice bred by Janvier Labs (Le Genest-Saint-Isle, France) were used. For each experiment, one week of adaptation of the animals to the environment was necessary before starting the procedure. MOS-J tumor cells were injected into various sites according to the template. All of the tumor cell injections were performed under general anesthesia (isoflurane 1.5% with air at 1 L/min) after disinfection with Betadine. All of the injections were performed within one hour of having harvested the cells. Preliminary experiments were performed to determine the optimal cell number to achieve reproducible kinetics and optimal growth.

Paratibial and intraosseous injections of MOS-J tumor cells were performed as described previously [10]. Briefly, for paratibial injection: 3.10^6 MOS-J cells were injected percutaneously into the middle diaphyseal tibia after periosteal denudation. Intraosseous injections were performed after a sub-centimetric inferio-lateral incision of the tibial tuberosity in order to expose the bone: the cortical bone was pierced with a needle by a rotational movement and then 3.10^6 MOS-J cells were injected. Doxorubicin treatment was initiated when the average tumor volume in one group exceeded 100 mm^3 as describe in the literature [10, 19, 20]. The intravenous injections were all performed biweekly in 50 µl of PBS with a solution of doxorubicin 4 mg/kg. The control group received injections of 50 µl PBS.

Histological characterization

Murine osteosarcoma models and sectioning: Three samples (from a group of six mice with median tumor volume) for each of the four groups were included in the study. The specimens were fixed in 4% formaldehyde for 24 hours, dissected, fixed another day at 4°C and decalcified in 4.13% EDTA, 0.2% paraformaldehyde, in 1× PBS buffer (pH 7.4) for 10 to 15 days at 50°C in a KOS microwave tissue processor (Milestone, MI, USA). The decalcified samples were then dehydrated by immersion in graded ethanol baths, cleared with 2-butanol, and embedded in paraffin. Ten serial 5-µm thick sections were cut from each sample at four levels separated by 250 µm in order to account for the tumor heterogeneity. The three first sections (sections 4-6) were immunostained for α-SMA, endomucin, and CD31 markers, while section 3 was triple-immunostained for CD31 and both endomucin and α-SMA markers.

Chromogenic immunohistochemistry: The sections were deparaffinized and subjected to 20 h of antigen retrieval in Tris-EDTA buffer (1 mM Tris, 0.5 mM EDTA, pH 9.0) at 60°C. The endogenous peroxidase activity was then blocked by incubating the sections with 3% H_2O_2, and non-specific binding was blocked with 2% normal donkey serum and 1% BSA in 1× Tris-buffered saline with 0.05% Tween 20, pH 7.4. Sections 4 to 6 of each of the four levels were then immunostained for CD31 (section 4), endomucin (section 5), and α-SMA (section 6), respectively. Briefly, after blocking, the sections were incubated for one hour at room temperature with rabbit ant-CD31 anti-

body (1:50; Abcam, ab28364), rat anti-endomucin antibody (1:50; Abcam, ab106100), and mouse anti-α-SMA antibody (1:3,000; R&D Systems, MAB1420). Immune complexes were visualized by the conventional ABC method using biotinylated donkey anti-rat (Jackson ImmunoResearch, 712-065-153), or donkey anti-mouse (Jackson ImmunoResearch, 715-065-151), or donkey anti-rabbit (Jackson ImmunoResearch, 711-065-152) secondary antibodies for 45 min followed by incubation with HRP (horseradish peroxidase)-streptavidin (Agilent, P0397) for another 45 min at room temperature. After staining with DAB liquid QUANTO substrate (MM France, F/TA-125-QHDX), the sections were counterstained with Gill-2 hematoxylin, dehydrated, cleared, and mounted with PERTEX® mounting medium (MM France, F/00811) and covered with a coverslip.

Triple-color immunofluorescence histochemistry: As for the chromogenic immunohistochemistry procedure, the sections were deparaffinized, subjected to 20 h of antigen retrieval in Tris-EDTA buffer (1 mM Tris, 0.5 mM EDTA, pH 9.0) at 60°C, and blocked with 2% normal donkey serum and 1% BSA in 1× Tris-buffered saline with 0.05% Tween 20, pH 7.4, to reduce non-specific binding. Sections 3 were immunostained with both rabbit anti-CD31 (1:40), rat anti-endomucin (1:50), and mouse anti-α-SMA (1:1,000) antibodies for an hour at room temperature. After three washes in 1× TBS-Tween 0.05%, pH 7.4, the following secondary antibodies were applied for another hour: Alexa Fluor® 488-conjugated donkey anti-rabbit (1:200; Jackson ImmunoResearch 711-545-152), biotinylated donkey anti-rat (1:200; Jackson ImmunoResearch 712-065-153), and Alexa Fluor® 647-conjugated donkey anti-mouse (1:200; Jackson ImmunoResearch 715-605-150). Finally, the sections were incubated with Cy3-conjugated streptavidin (1:400; Jackson ImmunoResearch 016-160-084) for one hour, and the nuclei were counterstained with DAPI (1:1,000; Thermo Fisher Scientific, D1306) and mounted with ProLong™ Gold Antifade reagent (Thermo Fisher Scientific, P36930) and covered with a coverslip.

Imaging and histomorphometry: Confocal images were obtained by using a Nikon AI N-SIM confocal microscope and subsequently treated by smoothing and noise reduction of each channel, followed by a Z-projection treatment using ImageJ software [21].

All of the histomorphometric analyses were conducted on scans of the immunostained sections. Acquisitions of sections 4-7 were made with a NanoZoomer Slide Scanner (Hamamatsu, Japan), and the images were then saved using NDP viewer software (Hamamatsu, version 2.2.6) at 5× magnification and exported at 10× using tiff format and analyzed with ImageJ software. Each of the chromogenically immunostained sections was individually analyzed on three specific regions of interest (ROI): one was defined by a representative 0.5-mm thick ROI for which the tumor tissue was along the bone; the other was a full representative picture of the core of the tumor; the last one was defined by a representative 0.5-mm thick ROI that contained the tumor invasion front. All of the analyses were carried out on each of the four levels of all of the samples. Briefly, the images were subjected to color deconvolution using the 'H-DAB' vector [22], thresholded, and non-specific noise was reduced. The results are presented as the mean value for each compartment of the number of positive elements per square millimeter.

For the triple-immunostained sections (section 3), the analysis was achieved using two levels that were considered, according to the results of those that had been obtained with the chromogenically immunostained sections, to be enough to yield consistent values. Quantification of the CD31+/α-SMA+ (mature vessels) and the CD31+/Endomucin+ (sinusoidal vessels) elements was carried out using a virtual microscope (NDP viewer) at a selected magnification of 20× on a representative field of 0.366 mm^2. Double-positive vessels were counted in the same manner as described above in the different compartments by selecting the two fluorochrome channels corresponding to the two markers of interest. The results are presented as the mean value of each level of each sample of double-positive elements per square millimeter.

Statistical analysis

The data were collected and analyzed using GraphPad Prism 7 software. Analysis of the results of the in vivo experiments between more than two distinct populations was per-

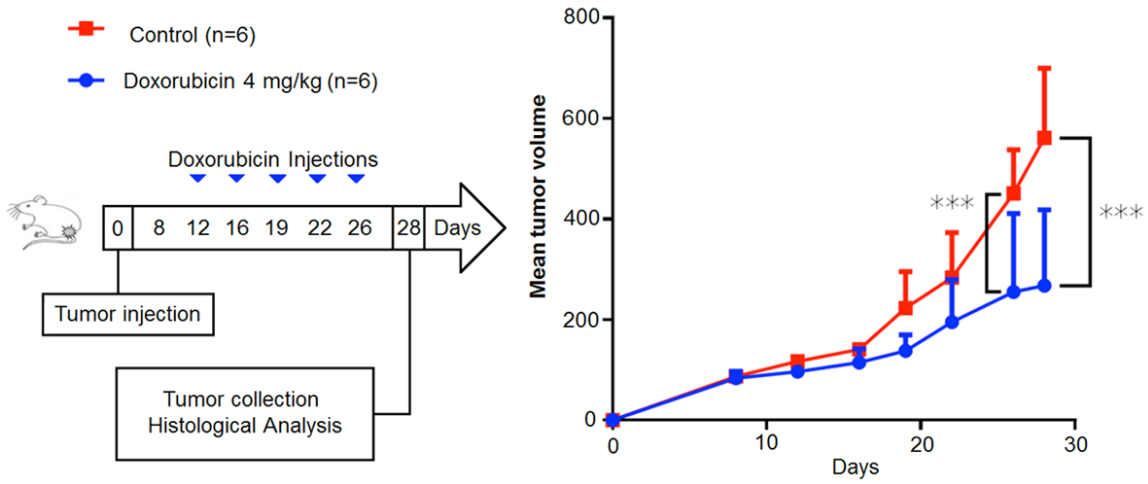

Figure 1. Effects of doxorubicin on MOS-J tumor growth. Injections of 4 mg/kg doxorubicin started at D12 and were repeated every 2 or 3 days. The tumor volumes were measured and expressed in mm^3. The results are expressed as means ± SD. n=6 in each group. Student's multiple *t*-tests. Threshold of significance: ***P≤0.001.

formed by one-way (only one condition tested) or two-way (two conditions tested) tests by applying the correction of the *Šidák* test for multiple comparisons. When two distinct groups were compared, we used the *t*-test with the Holm-*Šidák* correction method for multiple comparisons. The standard deviations are shown as numbers. The alpha risk for all these tests was set at 5%, with a significance of P<0.05.

Results

Effect of doxorubicin on the vascular signature in the OS mouse model

Validation of the effects of doxorubicin on primary tumor growth: We determined the effect of doxorubicin on tumor growth in the OS MOS-J mouse model, irrespective of the site of tumor initiation. Administration of doxorubicin started on Day 12 after tumor cell injection (**Figure 1**). As shown in **Figure 1**, no significant difference was observed for up to 26 days between the doxorubicin-treated and non-treated groups, although tumor volumes significantly decreased in the treated groups compared to the non-treated groups at 26 and 28 days (mean of the difference at 26 days: 196.2 mm^3, 95% CI [70.82 to 321.5], P<0.001, at 28 days: 293.9 mm^3, 95% CI [168.6 to 419.3], P<0.001) (Student's multiple *t*-tests).

Vascular markers in OS tumors in non-treated mice: We analyzed the vascular markers in the non-treated OS tumors. The selected markers were CD31, an endothelial marker; endomucin, which is expressed more specifically in high endothelial venules and in H-type vessels in bone; and α-SMA, which is a mural cell (pericyte and vascular smooth muscle cell) marker [16, 17, 23]. We decided to analyze CD31-positive (CD31+) and endomucin-positive (Endomucin+) elements, as they represent key endothelial structures of bone vasculature [16, 17]. α-SMA positive (-SMA+) staining was also chosen as it is linked to L-type vessels, which have been described in detail in the vascularization of bone [16, 18, 24]. α-SMA+ is a well-known marker of vascular maturity, with pericyte coverage of endothelial structures [24-26].

Our analysis aimed to integrate the cellular and the architectural features specific to bone tumors, and we, therefore, defined three geographic tumor areas in our study: the bone contact area with its periosteum, which is a niche for stem cells and vascularization [27-29] near the osteoblastic and osteoclastic activities; the invasion front, with potential leader cell phenotypes and highly proliferative capacities in direct contact with soft tissue [30, 31]; and the tumor center, which usually represents most of the necrotic area, with ischemic and metabolic features that are potential barriers for drug spread [10] (**Figure 2A**). Analysis of the vascular markers according to the different areas showed that endomucin+ elements/mm^2

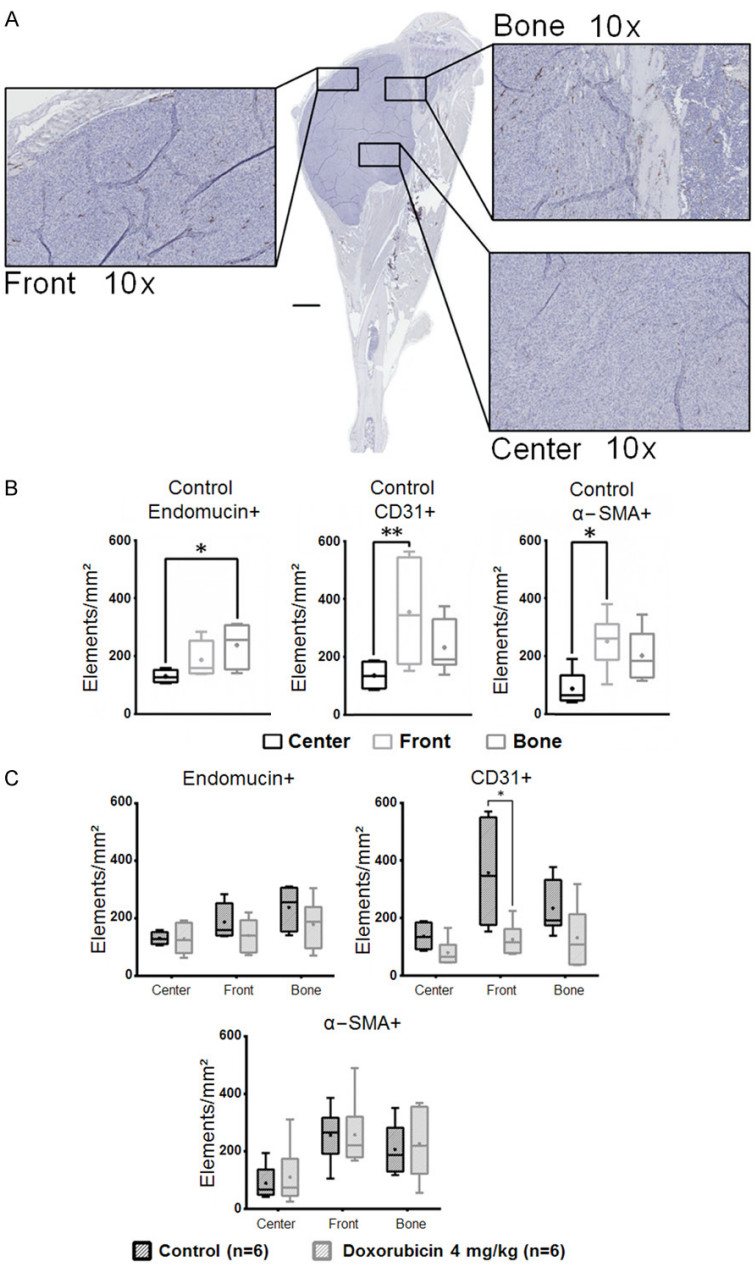

Figure 2. Vascular signature in the OS model determined by IHC staining. A: Expression of endomucin in distinct tumor areas (Front: invasion front; Bone: bone contact; Center: lesion center) evaluated by IHC staining. Image of an entire mouse leg (10x magnification; control group), the scale bar =1 mm; B: Histological analysis of endomucin, CD31, and α-SMA vascular markers in the control group. One-way ANOVA analysis, Thresholds of significance: *: [0.05; 0.01], **: [0.01; 0.001]; C: Effects of doxorubicin on the vascular signature in the selected tumor areas (Front: invasion front; Bone: bone contact; Center: lesion center). Box-plot with the minimal and the maximal values. The mean value is indicated by a dot. Two-way ANOVA analysis, Thresholds of significance: *: [0.05; 0.01], **: [0.01; 0.001].

were more abundant in the bone contact region compared to the lesion center (**Figure 2B**) (237.70±77.58 *vs.* 130.20±20.83, respectively, P=0.017). More CD31+ elements/mm^2 (136.50±44.61 *vs.* 357.1±180.97, P=0.002) and more α-SMA+ elements (90.32±57.74 *vs.* 256.30±92.31, P=0.029) were detected in the invasion front compared to the lesion center.

Expression of the vascular markers in OS tumors of doxorubicin-treated mice: In order to determine whether doxorubicin exposure could have an impact on the expression of vascular markers, we performed the same analysis on tumors from mice treated with doxorubicin. A significant decrease in CD31+ elements was observed in the invasion front (357.1±73.88 elements/mm^2 in the control group *vs.* 125.2±22.95 in the treated group, (P=0.031)), but not in the center nor in the bones of either group. There was also no significant difference in the number of endomucin+ or α-SMA+ elements between the control and the treated groups (**Figure 2C**).

Altogether, these results suggest that doxorubicin treatment is associated with a lower number of CD31+ elements in the invasion front of the tumor.

Analysis of the vascular network in tumors of non-treated and doxorubicin-treated mice: In order to obtain a more comprehensive view of the vascular network, we performed a multiplexed analysis to determine the CD31+/Endomucin+ and the CD31+/α-SMA+ elements, which are indicators of bone H-type vessels and mature vessels, respectively.

Confocal microscopy imaging (**Figure 3**) allowed for higher magnification and more precise visualization of the morphology of the CD31+/Endomucin+ and the CD31+/α-SMA+ elements

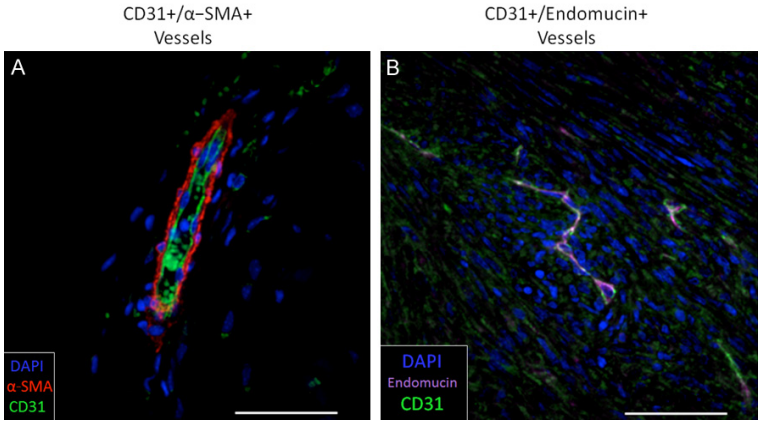

Figure 3. Confocal analysis of CD31+/α-SMA+ and CD31+/Endomucin+ co-staining in a control center lesion. A: CD31+/ α-SMA+ elements. B: CD31+/ Endomucin+ elements. The images are Z-stack projections at 63× magnification, the scale bars =20 µm. DAPI: nuclear staining.

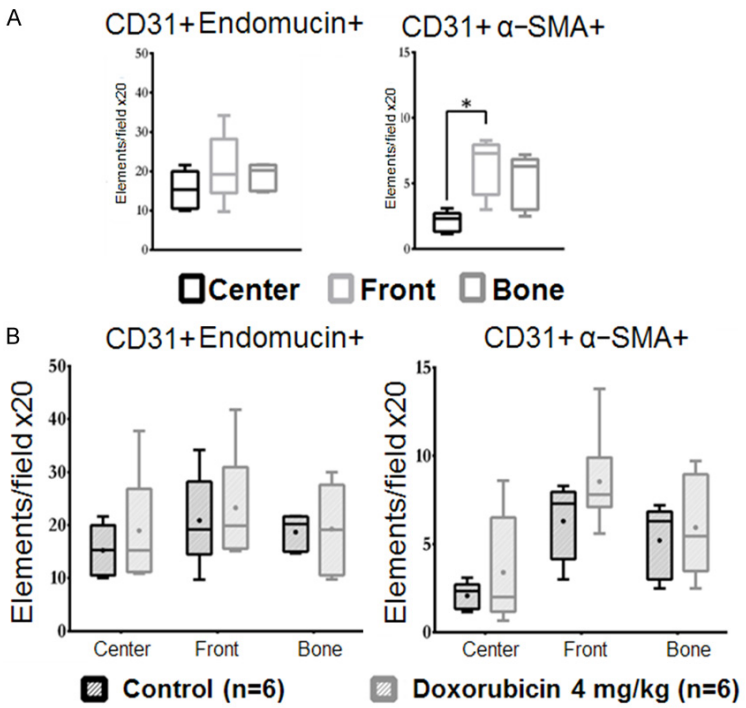

Figure 4. Vascular signature in the OS model determined by immunofluorescence double-staining of CD31+/Endomucin+ and CD31+/α-SMA+. Quantification of CD31+/Endomucin+ and CD31/α-SMA elements/field in defined tumor areas (center, front, bone). A: In the control group. B: In the control and the doxorubicin-treated group. Quantification was defined as elements/field at 20× magnification (lesion center, invasion front, and bone contact). Box-plot with the minimal and the maximal values, the mean value is indicated by a dot. Threshold of significance: P<0.01.

presented in **Figure 4**. Overall, the CD31+/α-SMA+ elements were well-defined, with a CD31+ endothelial inner part, and an α-SMA+ external mural/pericyte wall. They exhibited a structured and straight architecture, with a sizeable diameter, and they resembled mature vessels. On the other hand, the CD31+/Endomucin+ elements were much more sinusoidal, with a more serpiginous and unorganized structure. They also had a smaller diameter and they resembled immature sinusoidal vessels.

In the control group, more CD31+/α-SMA+ vessels were observed in the invasion front compared to the lesion center (6.30±2.16 elements/field *vs.* 2.08±0.77 elements/field, respectively, P=0.034) (**Figure 4A**). No significant differences were observed between the control and the doxorubicin-treated groups in the terms of the distribution of CD31+/Endomucin+ and the CD31+/α-SMA+ elements between the three different defined areas (**Figure 4B**).

Impact of the initial site of the tumor development on the vascular signature in treated mice

We then investigated whether the site of initiation of the tumor, namely paratibial *vs.* intraosseous, could impact the vascular signature of doxorubicin-exposed mice. To do so, we dichotomized the animal groups depending on their site of tumor injection. Analysis of the CD31+/α-SMA+ staining revealed that more CD31+/α-SMA+ elements were present in the treated tumors in the intraosseous model compared to the paratibial model (5.52± 3.23 elements/field *vs.* 1.27± 0.59, respectively, P=0.044, unpaired one-sided *t*-test) (**Figure 5A** and **5B**).

In regard to the tumor response to doxorubicin, significant differences were observed at Day 22, 26, and 28 depending on the tumor injection site (**Figure 5C**). In the intraosseous model, a better response to chemotherapy was

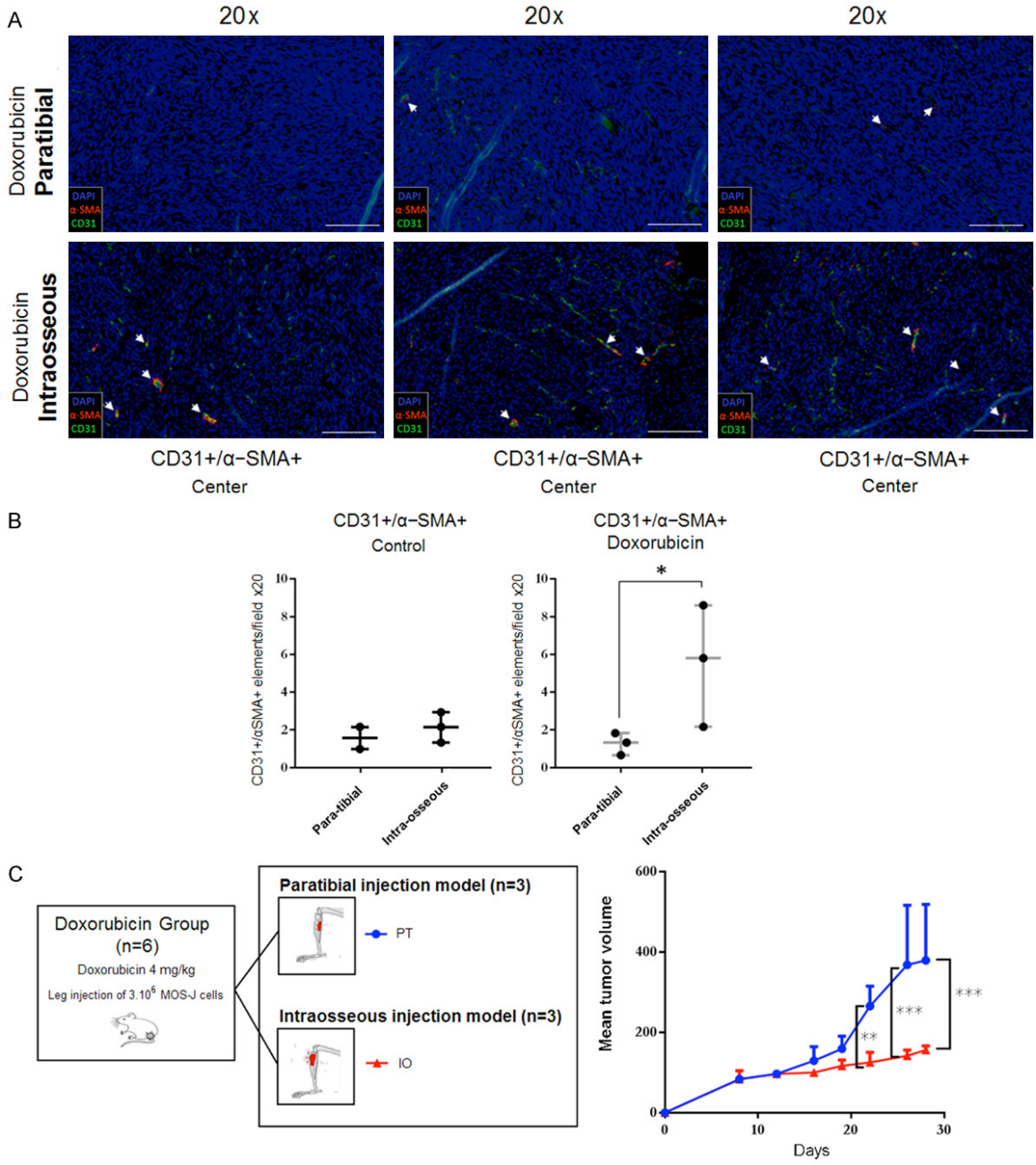

Figure 5. A: Vessel co-staining by immunofluorescence multiplexed for CD31+/α-SMA+ (20× magnification), the scale bar =100 µm. Images of control and doxorubicin-treated tumors for the paratibial and the intraosseous models. B: Histological analysis of control and doxorubicin-treated mouse vessels visualized by multiplexed CD31+/α-SMA+ immunofluorescence co-staining for the paratibial and intraosseous models. Quantification of elements/field at 20× magnification in the tumor center. Box-plot with the minimal and the maximal values, the mean value is indicated by a dot. Thresholds of significance: *: [0.05; 0.01]. Unpaired *t*-test one-sided. C: Increase in the average osteosarcoma volume in mice treated with doxorubicin (4 mg/kg), depending on the tumor initiation site (PT: Paratibial; IO: Intraosseous). The treatment was introduced at D12. Thresholds of significance: *: [0.05; 0.01], **: [0.01; 0.001], ***≤0.001. Student's multiple *t*-tests.

observed compared to the paratibial model, with a mean volume difference of 222.83 mm^3 at Day 28 (156.00 mm^3±10.39 *vs.* 378.83 mm^3±139.56, *t*-test; P<0.001, Student's multiple *t*-tests). These results were corroborated by the whole induced necrosis area percentage

analysis previously performed [10]; but we did not identify significant effect of Doxorubicin on Ki67 and Caspase3 staining on whole analysis (Supplementary Figure 1) [10]. The specific area analysis suggests that there were more CD31+/α-SMA+ mature vessels in the center of the tumors that responded well to doxorubicin in the intraosseous group, thus highlighting a potential vascular profile associated with a better response to chemotherapy.

Discussion

One of the most critical limitations in OS treatment is the high rate of relapse following a poor response to chemotherapy [8]. Predicting how each patient will respond to a specific chemotherapy regimen is a real challenge, and identifying factors predictive of a good response to better adjust chemotherapy protocols and improve OS survival rates remains an intensive field of research. Using a syngeneic mouse model of OS, we previously showed that the response to doxorubicin varies according to the site of tumor initiation [10]. The complexity of the bone tumor microenvironment could explain these differences. Although still poorly explored in OS, the vascular component is important as, aside from being a key factor for drug distribution [13, 32], it may also vary greatly depending on tumor angiogenesis and the nature of the tissue [16, 18, 33]. Furthermore, general and local treatments are thought to interact with the tumor and its environment, leading to a remodeling of the vascular system and eventually a normalization of the distribution and maturity of the vessels, thus improving drug distribution by a virtuous cycle [13, 34].

This study aimed to characterize the vascular environment in OS bone tumors and the effects of chemotherapy. Previously described in normal bone, we explored for the first time the expression of endomucin as a new vascular marker in bone tumor OS. Endomucin is an important endothelial marker in bone as it is highly co-expressed with CD31 in H-type vessels, which have been identified in various bone tissue locations such as the metaphysis near the growth plate and the endosteum. In normal growing bone, these vessels are responsible for mediating growth of the bone vasculature, maintaining perivascular osteoprogenitors, and coupling angiogenesis to osteogenesis [16, 35]. In the present study, we found that endomucin is also expressed in the syngeneic MOS-J model of OS, with fewer elements in the center of the lesion than in the area in contact with the bone. This is in agreement with the previous identification of abundant endomucin-positive elements in contact with active areas of bone remodeling [16-18].

A more detailed exploration of the vascular environment according to tumor territories was achieved by combining the endothelial markers endomucin and CD31 with the mural/pericyte marker α-SMA through a novel approach involving fluorescent multiplex immunohistochemistry. CD31/α-SMA-positive elements were significantly more abundant in the invasion front compared to the center of the tumor, in agreement with simple IHC staining showing an increase in CD31+ and α-SMA+ elements in this area. The confocal analysis highlighted the microvessel architecture and network organization. The CD31+/α-SMA+ elements were generally well defined, with a CD31+ endothelial inner part and an α-SMA+ external pericyte wall. These elements had a structured and straight architecture with a sizeable diameter and they are defined as mature vessels in the literature [36]. Pericytes support the structure and help stabilize blood vessels in addition to stimulating basement membrane production, thereby improving vasculature stability and permeability, which contribute to better tumor perfusion and hence the delivery of nutrients and O_2 as well as drugs and chemotherapy [37]. Importantly, these vessels are more abundant in the invasion front of tumors in mice, which is an area with a high degree of tumor cell proliferation and a high requirement for O_2 and nutrients. In contrast, the CD31+/Endomucin+ vessels in MOS-J tumor mice were of a small caliber, sinusoidal, and not continuous. These features are typical of angiogenic tumor microvessels, which are tortuous, leaky, and not surrounded by pericytes, and hence exhibit poor perfusion. We suspect that they have poor overall perfusion that resists blood flow and drug delivery in tumors. These functional characteristics of the tumor vasculature contribute to an elevated tumor interstitial fluid pressure that opposes diffusion and convection, which is the main form of transvascular transport of therapeutic agents in tumors [36]. These nonfunctional vessels may also underlie doxorubi-

cin resistance mechanisms, as a low degree of pericyte coverage may compromise vessel structure and functionality [38]. These anarchic vessels differ from the bulky and functional CD31+/αSMA+ vessels that can allow the diffusion of doxorubicin. Such characterization of vascular elements according to CD31, endomucin, and α-SMA co-staining has not been previously described in OS. Our methodology allowed us to clearly identify these two types of elements in different areas of the tumors, namely CD31+/Endomucin+ sprouting vessels and mature functional CD31+/α-SMA+ vessels.

Importantly, our results show that doxorubicin decreased the number of CD31+ elements present in the invasive front, without affecting the α-SMA- or endomucin-positive elements or the double-CD31/α-SMA-positive elements. It could illustrate a vascular pruning effect of doxorubicin, eliminating the most immature and unfunctional vessels first (CD31+, endomucin- and α-SMA-negative) [13]. Altogether, these results show that doxorubicin did not affect the repartition of CD31/α-SMA and CD31/Endomucin elements in the tumor areas. Thus, doxorubicin treatment does not appear to drastically alter the vascular signature in MOS-J OS tumors.

Despite our small cohort, encouraging results were obtained by an initial dichotomization of the animals between good responders to doxorubicin (intraosseous site of initiation) versus poor responders (paratibial site of injection). Indeed, we found a significant difference in the CD31+/αSMA+ mature vessels in the center part of the lesion, as they were four times more abundant in the good responding model compared to the poor responders [10]. This is in keeping with good tumor perfusion and drug delivery to the tumors as a result of mature vessels. These results open important perspectives for exploration of the vascular signature as a predictor of responses, which is a major current limitation for patients and clinicians.

Despite our small sample number, our study suggests that the mature vessels defined as CD31+/α-SMA+ elements, when they are present in the center of the lesion, may be considered to be markers of a good therapeutic response to doxorubicin This hypothesis needs to be explored further by analysis of a larger cohort and at the stage of tumor initiation using a dynamic approach. Analysis of human bone biopsies should also be considered for this specific marker in order to determine its potential as a predictor of a good response.

Our study is one of the first to specifically study the vascularization of OS by a multiplexed IF approach using a mouse preclinical model. Our methodology appears to be suitable for analyzing CD31+/α-SMA+ mature vessels with a pericyte coverage, as well as more immature CD31+/Endomucin+ sprouts of vascularization. Furthermore, this study opens new perspectives to more extensively explore the vascular microenvironment in OS.

Acknowledgements

We wish to thank the MicroPIcell platform (Stéphanie Blandin, Steven Nedellec, and Philippe Hulin). This work was supported by the Fondation pour la Recherche Médicale, FRM grant number DEA20150633177 awarded to Vincent Crenn. Experimental Therapeutic unit (Guylène Hamery, UTE Phan, IRS-UN, 8 quai Moncousu, BP70721, 44007 Nantes Cedex 1).

Disclosure of conflicts of interest

None.

Address correspondence to: Dr. Vincent Crenn, Nantes University, INSERM UMR 1238, Nantes, France. E-mail: vincent.crenn@chu-nantes.fr

References

[1] Ottaviani G and Jaffe N. The epidemiology of osteosarcoma. Cancer Treat Res 2009; 152: 3-13.

[2] Klein MJ and Siegal GP. Osteosarcoma anatomic and histologic variants. Am J Clin Pathol2006; 125: 555-581.

[3] Botter SM, Neri D and Fuchs B. Recent advances in osteosarcoma. Curr Opin Pharmacol 2014; 16: 15-23.

[4] Gibbs CP, Levings PP and Ghivizzani SC. Evidence for the osteosarcoma stem cell. Curr Orthop Pract 2011; 22: 322-326.

[5] Bielack SS, Kempf-Bielack B, Delling G, Exner GU, Flege S, Helmke K, Kotz R, Salzer-Kuntschik M, Werner M, Winkelmann W, Zoubek A, Jürgens H and Winkler K. Prognostic factors in high-grade osteosarcoma of the extremities or trunk: an analysis of 1,702 patients treated on neoadjuvant cooperative osteosarcoma study

group protocols. J Clin Oncol2002; 20: 776-790.
[6] Davis AM, Bell RS and Goodwin PJ. Prognostic factors in osteosarcoma: a critical review. J Clin Oncol 1994; 12: 423-431.
[7] Friebele JC, Peck J, Pan X, Abdel-Rasoul M and Mayerson JL. Osteosarcoma: a meta-analysis and review of the literature. Am J Orthop 2015; 44: 547-553.
[8] Gaspar N, Occean BV, Pacquement H, Bompas E, Bouvier C, Brisse HJ, Castex MP, Cheurfa N, Corradini N, Delaye J, Entz-Werlé N, Gentet JC, Italiano A, Lervat C, Marec-Berard P, Mascard E, Redini F, Saumet L, Schmitt C, Tabone MD, Verite-Goulard C, Le Deley MC, Piperno-Neumann S and Brugieres L; SFCE (Société Française des Cancers de l'Enfant et l'adolescent); GSF-GETO (Groupe Sarcome Français); UNICANCER Sarcoma Group. Results of methotrexate-etoposide-ifosfamide based regimen (M-EI) in osteosarcoma patients included in the French OS2006/sarcome-09 study. Eur J Cancer 2018; 88: 57-66.
[9] O'Kane GM, Cadoo KA, Walsh EM, Emerson R, Dervan P, O'Keane C, Hurson B, O'Toole G, Dudeney S, Kavanagh E, Eustace S and Carney DN. Perioperative chemotherapy in the treatment of osteosarcoma: a 26-year single institution review. Clin Sarcoma Res 2015; 5: 17.
[10] Crenn V, Biteau K, Amiaud J, Dumars C, Guiho R, Vidal L, Nail LL, Heymann D, Moreau A, Gouin F and Redini F. Bone microenvironment has an influence on the histological response of osteosarcoma to chemotherapy: retrospective analysis and preclinical modeling. Am J Cancer Res 2017; 7: 2333-2349.
[11] Corre I, Verrecchia F, Crenn V, Redini F and Trichet V. The osteosarcoma microenvironment: a complex but targetable ecosystem. Cells 2020; 9: 976.
[12] Hanahan D and Weinberg RA. The hallmarks of cancer. Cell 2000; 100: 57-70.
[13] Potiron V, Clément-Colmou K, Jouglar E, Pietri M, Chiavassa S, Delpon G, Paris F and Supiot S. Tumor vasculature remodeling by radiation therapy increases doxorubicin distribution and efficacy. Cancer Lett 2019; 457: 1-9.
[14] Dewhirst MW and Secomb TW. Transport of drugs from blood vessels to tumour tissue. Nat Rev Cancer 2017; 17: 738-750.
[15] Clere N, Renault S and Corre I. Endothelial-to-mesenchymal transition in cancer. Front Cell Dev Biol 2020; 8: 747.
[16] Kusumbe AP, Ramasamy SK and Adams RH. Coupling of angiogenesis and osteogenesis by a specific vessel subtype in bone. Nature 2014; 507: 323-328.
[17] Watson EC and Adams RH. Biology of bone: the vasculature of the skeletal system. Cold Spring Harb Perspect Med 2018; 8: a031559.
[18] Sivaraj KK and Adams RH. Blood vessel formation and function in bone. Development 2016; 143: 2706-2715.
[19] Ottewell PD, Mönkkönen H, Jones M, Lefley DV, Coleman RE and Holen I. Antitumor effects of doxorubicin followed by zoledronic acid in a mouse model of breast cancer. J Natl Cancer Inst 2008; 100: 1167-1178.
[20] Sommer K, Peters SO, Robins IH, Raap M, Wiedemann GJ, Remmert S, Sieg P, Bittner C and Feyerabend T. A preclinical model for experimental chemotherapy of human head and neck cancer. Int J Oncol 2001; 18: 1145-1149.
[21] Schneider CA, Rasband WS and Eliceiri KW. NIH image to ImageJ: 25 years of image analysis. Nat Methods 2012; 9: 671-675.
[22] Landini G, Martinelli G and Piccinini F. Colour deconvolution-stain unmixing in histological imaging. Bioinformatics 2021; 37: 1485-1487.
[23] Kanda H, Tanaka T, Matsumoto M, Umemoto E, Ebisuno Y, Kinoshita M, Noda M, Kannagi R, Hirata T, Murai T, Fukuda M and Miyasaka M. Endomucin, a sialomucin expressed in high endothelial venules, supports L-selectin-mediated rolling. Int Immunol 2004; 16: 1265-1274.
[24] Alarcon-Martinez L, Yilmaz-Ozcan S, Yemisci M, Schallek J, Kılıç K, Can A, Di Polo A and Dalkara T. Capillary pericytes express α-smooth muscle actin, which requires prevention of filamentous-actin depolymerization for detection. Elife 2018; 7: e34861.
[25] Bergers G and Song S. The role of pericytes in blood-vessel formation and maintenance. Neuro Oncol 2005; 7: 452-464.
[26] Chang L, Scott MA, Meyers CA and James AW. Pericytes in sarcomas and other mesenchymal tumors. Adv Exp Med Biol 2019; 1147: 109–124.
[27] Chanavaz M. The periosteum: the "umbilical cord" of bone. Quantification of the blood supply of cortical bone of periosteal origin. Rev Stomatol Chir Maxillofac 1995; 96: 262-267.
[28] Mahajan A. Periosteum: a highly underrated tool in dentistry. Int J Dent 2012; 2012: 717816.
[29] Moore SR, Heu C, Yu NYC, Whan RM, Knothe UR, Milz S and Knothe Tate ML. Translating periosteum's regenerative power: insights from quantitative analysis of tissue genesis with a periosteum substitute implant. Stem Cells Transl Med 2016; 5: 1739-1749.
[30] Yong KMA, Li Z, Merajver SD and Fu J. Tracking the tumor invasion front using long-term fluidic tumoroid culture. Sci Rep 2017; 7: 1-7.
[31] Aw Yong KM, Ulintz PJ, Caceres S, Cheng X, Bao L, Wu Z, Jiagge EM and Merajver SD. Heterogeneity at the invasion front of triple negative breast cancer cells. Sci Rep 2020; 10: 5781.

[32] Primeau AJ, Rendon A, Hedley D, Lilge L and Tannock IF. The distribution of the anticancer drug doxorubicin in relation to blood vessels in solid tumors. Clin Cancer Res 2005; 11: 8782-8788.
[33] Kusumbe AP. Vascular niches for disseminated tumour cells in bone. J Bone Oncol 2016; 5: 112-116.
[34] Clément-Colmou K, Potiron V, Pietri M, Guillonneau M, Jouglar E, Chiavassa S, Delpon G, Paris F and Supiot S. Influence of radiotherapy fractionation schedule on the tumor vascular microenvironment in prostate and lung cancer models. Cancers 2020; 12: 121.
[35] Xie H, Cui Z, Wang L, Xia Z, Hu Y, Xian L, Li C, Xie L, Crane J, Wan M, Zhen G, Bian Q, Yu B, Chang W, Qiu T, Pickarski M, Duong LT, Windle JJ, Luo X, Liao E and Cao X. PDGF-BB secreted by preosteoclasts induces CD31hiEmcnhi vessel subtype in coupling osteogenesis. Nat Med 2014; 20: 1270-1278.
[36] Bhattacharya A, Seshadri M, Oven SD, Tóth K, Vaughan MM and Rustum YM. Tumor vascular maturation and improved drug delivery induced by methylselenocysteine leads to therapeutic synergy with anticancer drugs. Clin Cancer Res 2008; 14: 3926-3932.
[37] Ruoslahti E. Specialization of tumour vasculature. Nat Rev Cancer 2002; 2: 83-90.
[38] Ribeiro AL and Okamoto OK. Combined effects of pericytes in the tumor microenvironment. Stem Cells Int 2015; 2015: 868475.

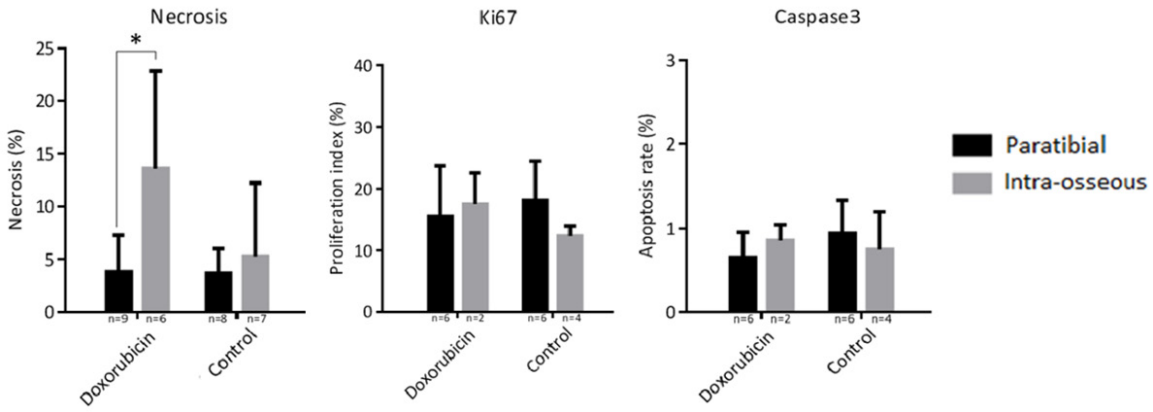

Supplementary Figure 1. Histological whole analysis of induced necrosis from previous experiments on same mice specimen (percentage of necrosis relative to the tumor area), cell proliferation with IHC labeling of Ki67 (expressed as a proliferation index), and apoptosis with IHC cell labeling of caspase 3. Thresholds of significance: * [0.05; 0.01], ** [0.01; 0.001], *** ≤0.001 (11).